Desroches, M. F., Krauskopf, B., & Osinga, H. M. (2008). The geometry of mixed-mode oscillations in the Olsen model for peroxidase-oxidase reaction.

The geometry of mixed-mode oscillations in the Olsen model for Peroxidase-Oxidase reaction

Mathieu Desroches, Bernd Krauskopf and Hinke M. Osinga

Bristol Center for Applied Nonlinear Mathematics

Department of Engineering Mathematics

University of Bristol, Queen's Building, Bristol BS8 1TR, UK

Preprint of September 12, 2008

2000 MSC: Primary: 58F15, 58F17; Secondary: 53C35
Keywords: mixed-mode oscillations, delayed Hopf bifurcation, invariant manifolds

Abstract

We study the organization of mixed-mode oscillations (MMOs) in the Olsen model for peroxidase-oxidase reaction. This model is a four-dimensional slow-fast system, but it does not have a clear split into slow and fast variables. A numerical continuation study shows that the MMOs appear as families in a complicated bifurcation structure that involves many regions of multistability. We show that the small-amplitude oscillations of the MMOs arise from the slow passage through a (delayed) Hopf bifurcation of a three-dimensional fast subsystem, while large-amplitude excursions are due to a global reinjection mechanism. To characterize these two key components of MMO dynamics geometrically we consider attracting and repelling slow manifolds in phase space. More specifically, these objects are surfaces that are defined and computed as one-parameter families of stable and unstable manifolds of saddle equilibria of the fast subsystem. The attracting and repelling slow manifolds interact near the Hopf bifurcation, but also explain the geometry of the global reinjection mechanism. Their intersection gives rise to canard-like orbits that organize the spiralling nature of the MMOs.

1 Introduction

The peroxidase-oxidase (PO) reaction is a famous biochemical experiment that displays nonlinear dynamics, including bistability and chaos. In the experimental set-up two substrates, reduced nicotinamide adenine dinucleotide ($NADH$) and oxygen from a N_2/O_2 gas phase are pumped at a constant rate into a reaction mixture containing horseradish peroxidase. The enzyme peroxidase acts as a catalyst to oxidise $NADH$ via molecular oxygen. The net overall reaction is given by

$$O_2 + 2NADH + 2H^+ \rightarrow 2H_2O + 2NAD^+,$$

Table 1: Values of the parameters of the Olsen model (1)–(4)

k_1	k_2	k_3	k_4	k_5	k_6	k_7	k_{-7}	k_8	α
0.34	250	0.035	20	5.35	10^{-5}	0.8	0.1	0.825	1

but it is known that the reaction is a branched chain reaction that involves at least two intermediate free radicals. There is no universally agreed mathematical model for this reaction, but the simplest model involves the two substrates O_2 denoted A and $NADH$ denoted B and two free radicals X and Y. This four-dimensional model was introduced by Degn, Olsen and Perram in [9] and later modified by Olsen [28] to include the possibility for chaotic dynamics. It is now known as the Olsen model and it is given by the differential equations

$$\dot{A} = -k_3ABY + k_7 - k_{-7}A, \tag{1}$$
$$\dot{B} = \alpha(-k_3ABY - k_1BX + k_8), \tag{2}$$
$$\dot{X} = k_1BX - 2k_2X^2 + 3k_3ABY - k_4X + k_6, \tag{3}$$
$$\dot{Y} = -k_3ABY + 2k_2X^2 - k_5Y. \tag{4}$$

Here, we introduced the parameter α for the purposes of this paper and normally $\alpha = 1$. The other nine parameters are reaction rates. We remark that k_6 in equation (3) is a small parameter that accounts for the spontaneous (slow) formation of free radicals; if $k_6 = 0$ then the reaction does not start in a real experiment. The parameter k_1 is linearly related to the enzyme concentration and typically serves as the main bifurcation parameter; also k_5 and k_2 have been used as bifurcation parameters [1].

The PO reaction has been studied extensively since the middle of the 1960s [32] and a range of interesting dynamical phenomena have been observed. In particular, the experiment can exhibit mixed-mode oscillations (MMOs), that is, periodic motion that consist of both small- and large-amplitude oscillations. The Olsen model is remarkably good at reproducing all experimental observations, although numerical studies have also been based on more detailed higher-dimensional models. Numerical studies (by means of simulation of the model equations) particularly focused on bistability of steady states and/or (mixed-mode) periodic orbits [3, 20, 21, 22, 29, 30]. Different scenarios have been proposed to explain possible routes to chaos: break-up of invariant tori [21], cascades of period-doubling and period-adding bifurcations [14, 30], and also homoclinic chaos [13]. All these different routes to chaos are organized via sequences of MMOs.

The most interesting feature of the Olsen model is the fact that the dynamics of (1)–(4) is slow-fast in nature, but the equations do not allow for a straightforward split into slow and fast variables. As a result, it is very hard to extract the geometry that organizes the MMOs. Observations from experiments and simulation have led to the generally accepted view that B evolves on a slower timescale than the other reactants [22, 30]. In this paper we make use of this property, which allows one to explained the dynamics of (1)–(4) by considering the three-dimensional fast subsystem, where B is a parameter, that is, $\alpha = 0$ in (2).

This paper is motivated directly by the work of Brøns and Krupa [5, 19] who considered the Olsen model (1)–(4) with the parameter values given in Table 1 that are also used here. With the exception of the value for k_1, these parameters were all already proposed in [1, 28]. The main question is how MMOs arise in the Olsen model, and canard phenomena associated

with folded singularities have been suggested as their source [5, 19]; see also [18]. We find that the geometry of MMOs in the full system is organized by a strong contraction, followed by slow passage through a delayed Hopf bifurcation of the fast subsystem; see section 3. The actual period of a mixed-mode oscillation is determined by a reinjection mechanism that brings the trajectory back to the vicinity of the Hopf bifurcation. The concepts of strong contraction, slow passage through a Hopf bifurcation and a reinjection mechanism are also identified in [23, 24] to explain the generation of MMOs in a three-dimensional system. The added difficulty here is that the Olsen model is of dimension four. We remark that X is known to be a particularly fast variable that is often eliminated from the equation via a quasi steady-state assumption to simplify the analysis [11]. By contrast, we find that the dynamics of X plays an essential role in the reinjection. Hence, the geometry of phase space proposed here gives a truly four-dimensional insight.

Inspired by previous work [4, 7, 8, 31] on slow-fast dynamical systems in $\mathbb{R}^3$ with two slow variables, our main aim is to seek equivalents of locally attracting and repelling slow manifolds that organize phase space. This approach is similar in spirit to [33], but we cannot make use of an explicit splitting into slow and fast variables. The reduction methods in [6] do not depend on an explicit splitting, but use the dominant time scales along the attracting orbit to select a sequence of reduced models that are valid along finite time segments. Our goal is to find a geometric split of phase space that suggests appropriate reductions more globally and not only along an attractor. To this end, we first compute a detailed bifurcation diagram of mixed-mode periodic orbits. As in [5, 19] we vary k_5 as the main bifurcation parameter, which corresponds to the rate at which Y is transformed into a nonreactive product. The overall bifurcation structure we find consists of accumulating isolas of different MMOs. In particular, we find numerous instances of coexisting mixed-mode periodic attractors in the Olsen model (1)–(4), which to our knowledge has not been reported before. We also show that the bifurcation structure (including multistability of MMOs) does not change in an essential way when $k_6 = 0$. We proceed by finding slow manifolds as stable and unstable manifolds of saddle equilibria of the slow system, where we make use of the fact that the (A, B)-plane is invariant for $k_6 = 0$. The slow manifolds we consider are two-dimensional surfaces that can be computed as one-parameter families of suitable orbit segments; see also [17]. The attracting and repelling slow manifolds interact in the vicinity of the delayed Hopf bifurcation, but extend throughout phase space so that they capture the reinjection mechanism as well. The number of small oscillations during the transition through the delayed Hopf bifurcation can be described by canard-like orbits.

This paper is organized as follows. In the next section we present a detailed bifurcation diagram of mixed-mode periodic orbits in the bifurcation parameter k_5, and we present numerical evidence that this bifurcation structure persists also when $k_6 = 0$. Section 3 focuses on the three-dimensional fast subsystem where $\alpha = 0$, specifically on its equilibria and their stability. This information is used in section 4 to define and compute attracting and repelling slow manifolds. Canard-like orbits that describe the interaction of the two slow manifolds are the subject of section 5. Finally, section 6 discusses the results with emphasis on avenues for future work.

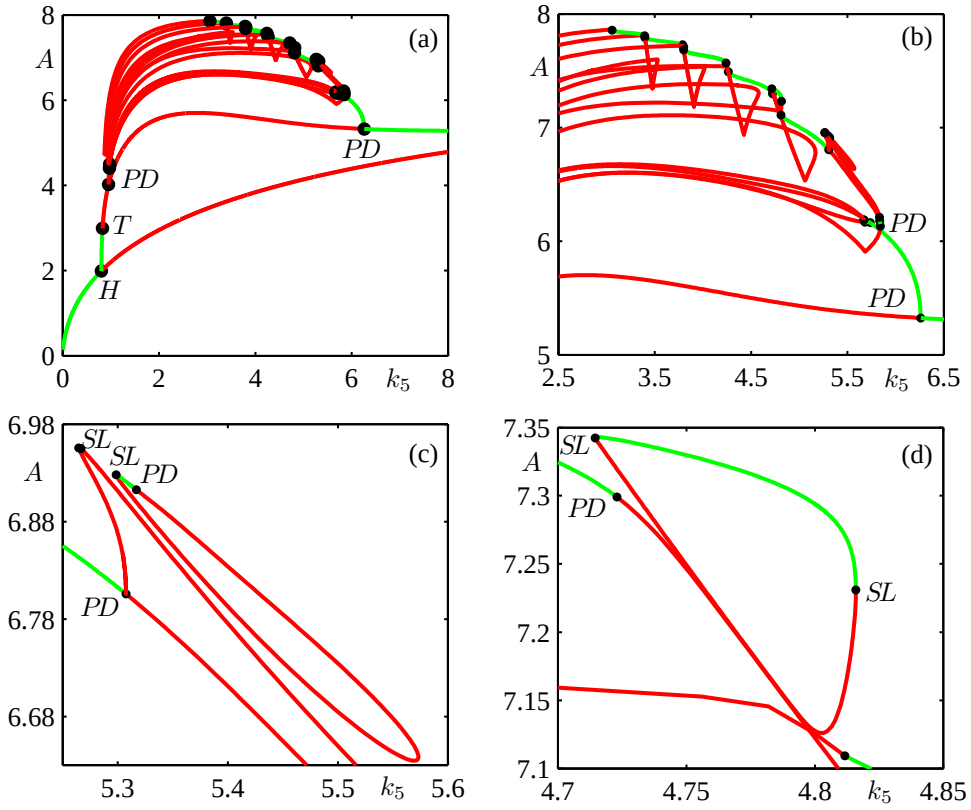

Figure 1: Bifurcation diagram of (1)–(4) as a function of k_5, where all other parameters are as in Table 1. Panel (a) shows the overall bifurcation structure in the range $k_5 \in [0, 8]$ and panel (b) an enlargement. Panels (c) and (d) show isolas of periodic orbits near $k_5 = 5.3$ and $k_5 = 4.8$, respectively. Stable parts of branches are green and unstable ones red; branches bifurcate at points of Hopf (H), saddle-node of limit cycle (SL), period-doubling (PD), and torus (T) bifucations.

2 Bifurcation structure of periodic orbits

As a starting point of our analysis, we determine (with the software package AUTO [2]) the bifurcation diagram of the four-dimensional Olsen model (1)–(4) as a function of the parameter k_5. We first consider the values of the parameters in Table 1, and then show that the bifurcation structure of periodic orbits persists for the limiting case where $k_6 = 0$. In particular, we find a considerable amount of multistability between different types of periodic orbits.

2.1 Bifurcation diagram for standard parameter values

Figure 1 shows the bifurcation diagram of (1)–(4) when k_5 is varied, where the value of the variable A is used in the representation. All other parameters are as in Table 1 and, in particular, k_6 has its standard value of $k_6 = 10^{-5}$. Panel (a) illustrates the overall bifurcation structure in the interval $[0, 8]$. A unique stationary solution of (1)–(4) is stable for low k_5

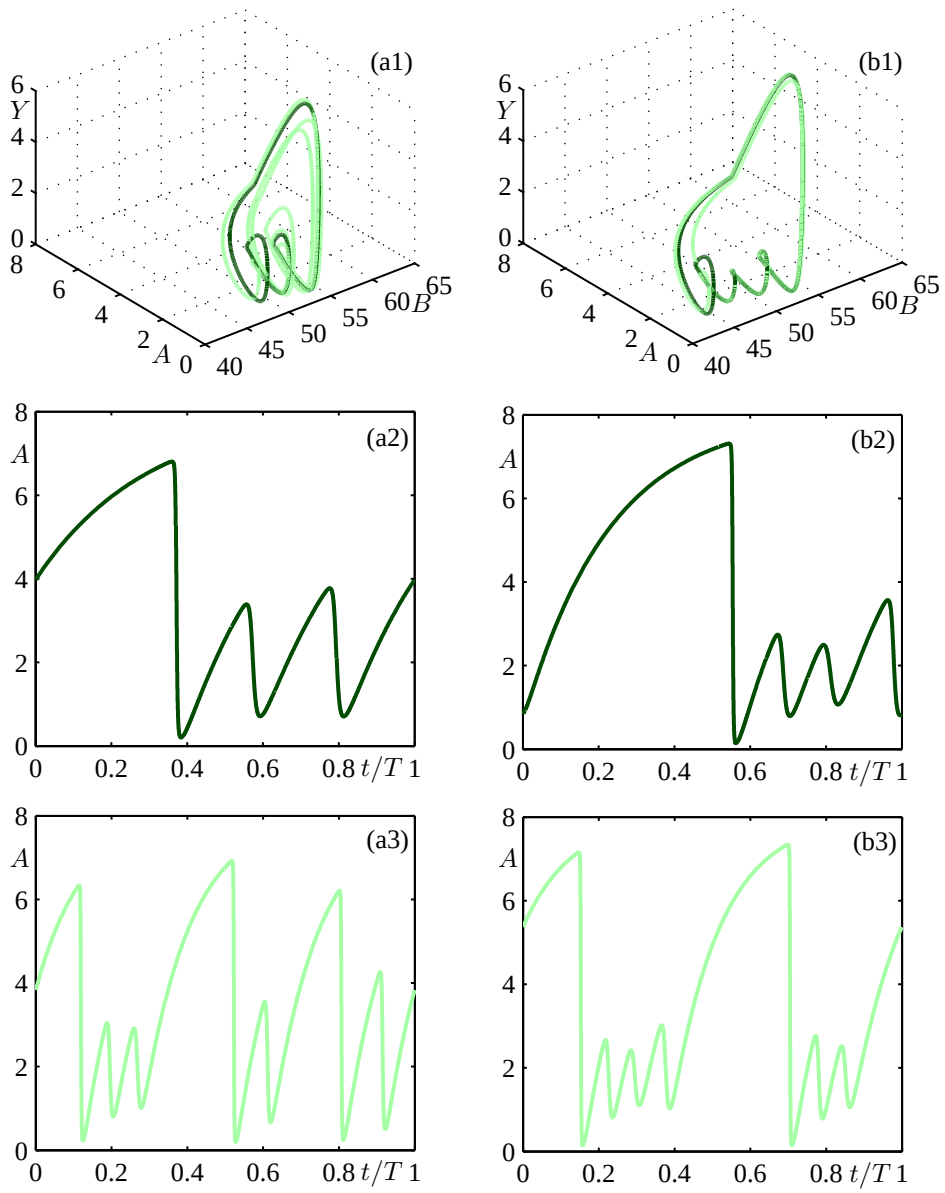

Figure 2: Pairs of coexisting attracting periodic orbits for $k_5 = 5.305$ (a1)–(a3) and $k_5 = 4.713$ (b1)–(b3) with all other parameters as in Table 1; compare with Figure 1. Panels (a1)/(b1) show the respective two periodic orbits in (A, B, Y)-space, while (a2)/(b2) and (a3)/(b3) show their time profiles.

and loses its stability at a supercritical Hopf bifurcation H at $k_5 \approx 0.804$. From the point H emanates a branch of basic periodic orbits; they are initially stable and lose their stability at $k_5 \approx 0.828$ in a torus (or Neimark-Sacker) bifurcation T. This branch of (now unstable) periodic orbits undergoes a period-doubling bifurcation PD at $k_5 \approx 0.954$ and restabilizes at a second period-doubling bifurcation PD at $k_5 \approx 6.26$; it exists stably until $k_5 \approx 25.07$ where a second (subcritical) Hopf bifurcation (not shown) marks the end of the oscillatory

region for k_5. The period-doubling point *PD* at $k_5 \approx 6.26$ is the starting point of a cascade of period-doublings (for decreasing k_5) of the family of basic periodic orbits. All (eventually unstable) branches emerging from this period-doubling cascade can be continued to another period-doubling cascade starting from the point *PD* at $k_5 \approx 0.954$.

What is more, we find a sequence of isolas (closed branches), which in turn give rise to new cascades of period-doublings and further isolas. Note that finding isolas is rather difficult because of the need to find an initial periodic orbit on the respective isola. We managed to find six large isolas and three small isolas in total, by employing a combination of systematic searching via numerical integration from suitable initial conditions and the continuation of selected branches. In Figure 1(a) and (b) six large isola are shown; note that it is hard to distinguish individual isolas due to the projection onto the (k_5, A)-plane. The first and largest isola extends from near the period-doubling cascade at $k_5 \approx 6.26$ all the way to near the left-most period-doubling bifurcation *PD* at $k_5 \approx 0.954$. On this first isola we find a period-doubling bifurcation *PD* at $k_5 \approx 5.84$, which in turn is the beginning of a period-doubling cascade of stable periodic orbits; see Figure 1(b). Similarly, a new large isola can be found near a period-doubling cascade of stable periodic orbits on a previous large isola. All large isolas extend to very near the left-most period-doubling bifurcation *PD* at $k_5 \approx 0.954$. Figure 1(c) and (d) shows that there are also small isolas, locally near period-doubling cascades of large isolas. In both cases part of the isola corresponds to attracting periodic orbits. The stable periodic orbits on small isolas lose their stability either in saddle-node of limit cycle (*SL*) or in period-doubling bifurcations.

Importantly, stable segments on isolas are responsible for a considerable amount of multistability between different periodic orbits in the Olsen model. Bistability between coexisting stable fixed points has been reported in some experimental and simulation studies of the PO reaction [3, 30] but, to our knowledge, coexisting stable MMOs have not been found previously in the Olsen model. Figure 2 shows two example of pairs of simultaneously stable MMOs for $k_5 = 5.305$ and $k_5 = 4.713$, respectively. This choice of k_5 corresponds to the stable parts of the two small isolas in Figure 1(b) and (c), which overlap in k_5 with stable segments of two large isolas. The three-dimensional views of the pairs of periodic orbits in (A, B, Y)-space in panels (a1)/(b1) are accompanied by time series of the variable A over one period in panels (a2)/(b2) and (a3)/(b3); here the periodic orbits from the large isolas appear in dark colors and those from the small isolas in light colors. The MMO pattern of large and small oscillations per period shows that the (dark) orbits associated with the large isolas have a less elaborate MMO pattern than the (light) orbits associated with the small isolas.

2.2 The limiting case of $k_6 = 0$

The standard value $k_6 = 10^{-5}$ is very small, so that it appears natural to make use of special properties of system (1)–(4) for $k_6 = 0$. The first step is, therefore, to check what happens to the bifurcation structure of mixed-mode periodic orbits that we found in the previous section if we replace $k_6 = 10^{-5}$ with $k_6 = 0$.

Figure 3 confirms that one still finds all the richness of the underlying bifurcation structure for $k_6 = 0$. Specifically, the bifurcation diagram in panel (a) has the same overall structure and qualitative features as that for $k_6 = 10^{-5}$. The branch of equilibria and the

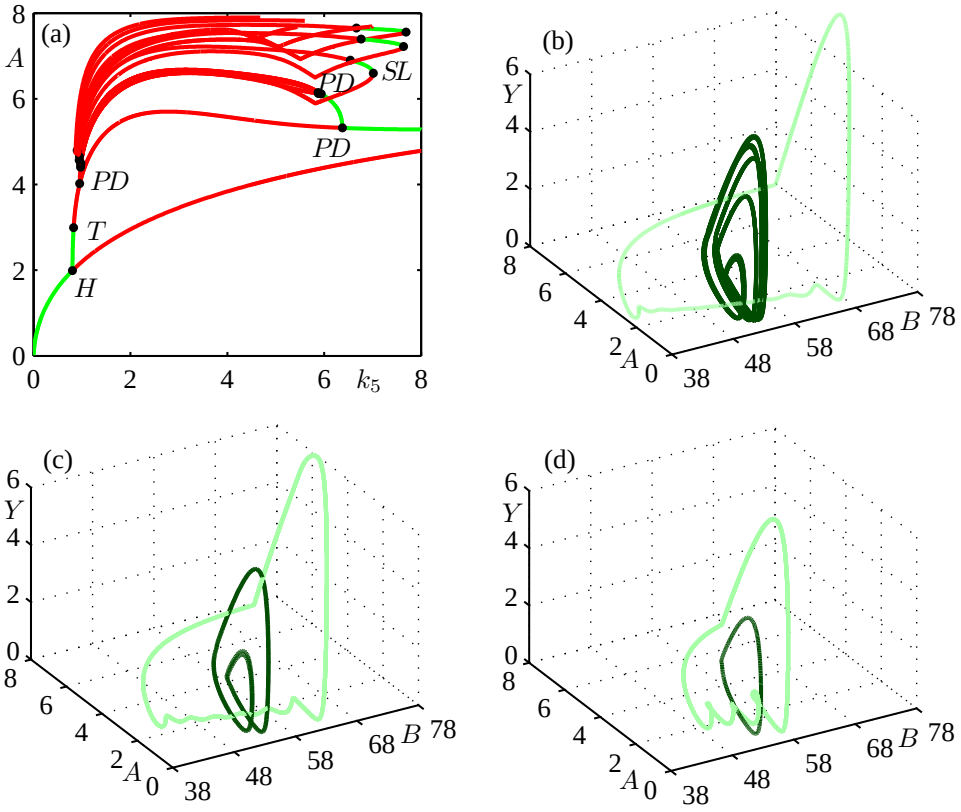

Figure 3: Bifurcation diagram (a) of (1)–(4) for $k_5 \in [0, 8]$, where $k_6 = 0$ and all other parameters are as in Table 1; compare with Figure 1. Panels (b)–(d) are examples of pairs of coexisting periodic attractors for $k_5 = 5.93$, $k_5 = 6.0$ and $k_5 = 6.82$, respectively.

basic branch of periodic orbits that bifurcate from it at the Hopf point H are virtually unchanged; compare with Figure 1(a). Furthermore, the isolas of mixed-mode periodic orbits also persist and they accumulate in the same way near the left-most period-doubling point PD. A difference is that the large islands and their stable parts extend further to the right, past the right-most period-doubling bifurcation PD. The right endpoints of the large isolas are saddle-node of limit cycle bifurcations that also determine one boundary of the stable part of the isola. While the calculations are quite delicate, our numerical evidence suggests that these points are increasingly sharp folds that appear to accumulate near $\{A = 8\}$. Overall, we still find multistability between different MMOs, but shifted towards larger values of k_5. Three examples of pairs of coexisting attracting orbits are shown in Figure 3(b)–(d). The panels show in (A, B, Y)-space mixed-mode periodic orbits with a single large peak and several small peaks (light color). Other mixed-mode periodic orbits coexist containing a total of eight, two and one peaks, respectively (dark color). These smaller orbits can be found by numerical continuation along the period-doubling cascade of basic periodic orbits. Note that Figure 3(b) is for the standard parameter value of $k_5 = 5.35$ as given in Table 1. While the period-two orbit and the period-one orbit in panels (c) and (d) are stable, the period-eight orbit in panel (b) is already unstable for $k_5 = 5.35$. This agrees with the obser-

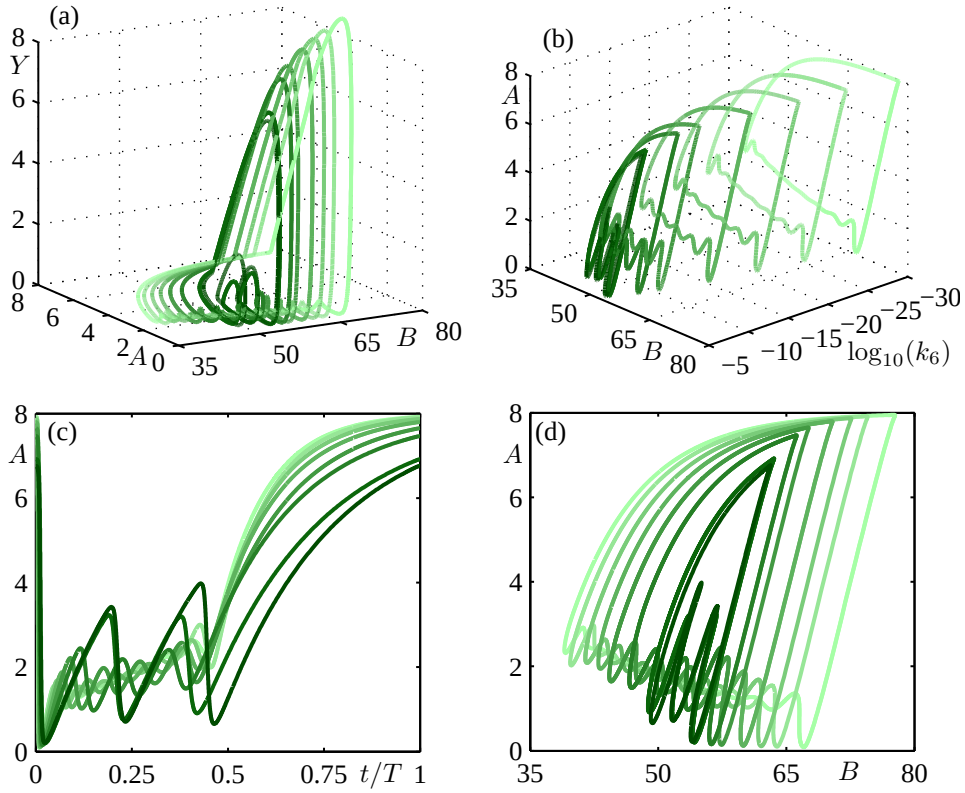

Figure 4: Stable mixed-mode periodic orbits for $k_6 \in [0, 10^{-5}$, shown in (A, B, Y)-space (a), in $(\log_{10}(k_6), A, Y)$-space (b), as time series over one period (c), and in projection onto the (A, B)-plane (d); the color changes gradually from light for $k_6 = 0$ to dark for 10^{-5}.

vation reported in [1] that the standard value of k_1 lies very near the boundary of a region of nonperiodic and chaotic oscillations (for both $k_6 = 10^{-5}$ and $k_6 = 0$, and for $k_5 = 5.35$).

Figure 4 shows stable mixed-mode periodic orbits of system (1)–(4) as a function of k_6, of which the individual panels show different representations. These stable orbits are found by numerical integration from the previous attractor. Note that there is a single large peak throughout, while the number of small oscillations of the orbit decreases with increasing k_6; see Figure 4(c) and (d). One finds stable mixed-mode periodic orbits up to $k_6 \approx 8.95 \times 10^{-6}$. The final (darkest) periodic orbit in Figure 4 for $k_6 = 10^{-5}$ is actually very weakly unstable; it has been found by continuation from the last stable orbit.

3 Bifurcations of the fast subsystem

The variable B evolves on a slower time scale than the other variables in the Olsen model (1)–(4). Therefore, the bifurcations of the fast subsystem, the limit where B does not change at all, are important for understanding the overall dynamics. The fast subsystem is given by setting $\alpha = 0$ in (2), which means that $\dot{B} = 0$ so that B becomes a parameter in the equations for A, X and Y.

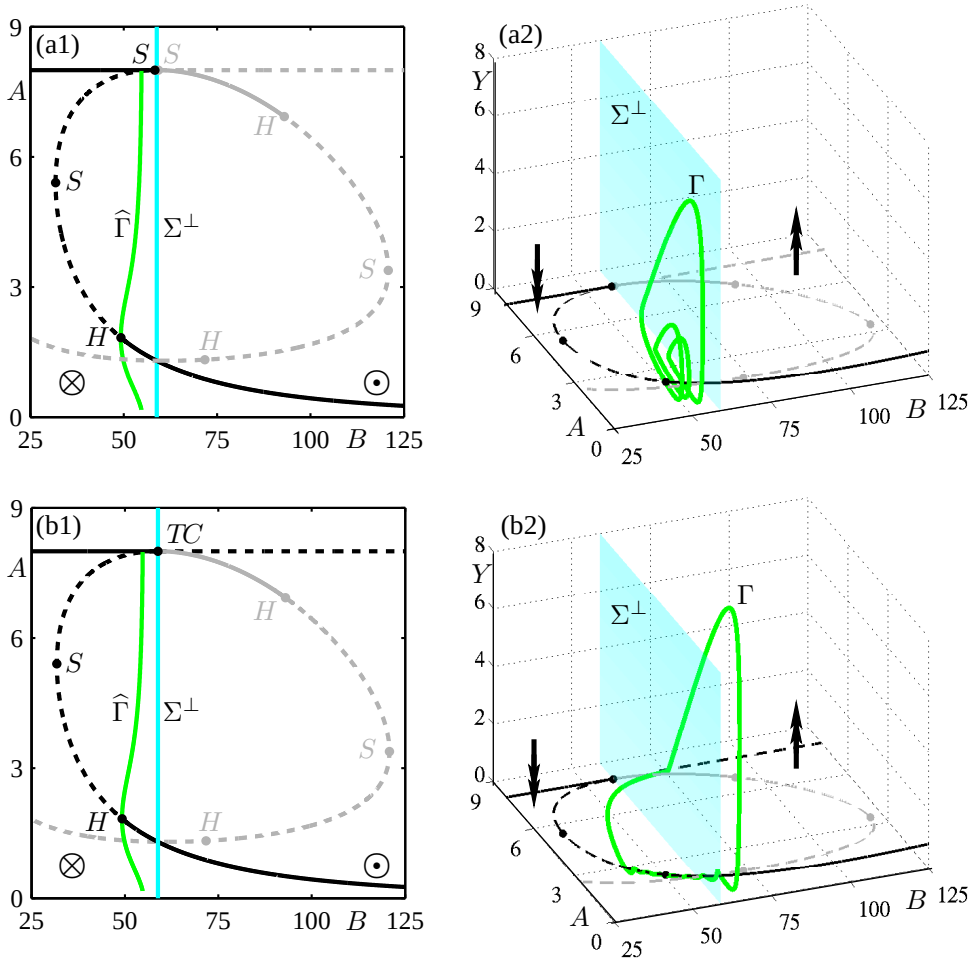

Figure 5: Bifurcation diagram of the fast subsystem, system (1)–(4) with $\alpha = 0$ where B is a parameter, for $k_6 = 10^{-5}$ (a) and $k_6 = 0$ (b). Panels (a1)/(b1) show branches of equilibria (A, B)-plane, which undergo saddle-node (S), Hopf (H) and transcritical (TC) bifurcations; stable equilibria are represented by solid and unstable ones by dashed curves. Also shown is the family $\widehat{\Gamma}$ of periodic orbits (green curve) that bifurcates form the Hopf point H. Panels (a2)/(b2) show the equilibrium branches in (A, B, Y)-space together with the respective mixed-mode periodic orbit from Figure 4 (which exists for $\alpha = 1$). At the cyan line/plane $\Sigma^{\perp}$ the flow normal to the (A, B)-plane changes direction as indicated by the arrow symbols.

Figure 5 presents the bifurcation diagram of the fast subsystem for $k_6 = 10^{-5}$ and for $k_6 = 0$, respectively. Panels (a1)/(b1) show branches of equilibria and a bifurcating family $\widehat{\Gamma}$ of periodic orbits in the (A, B)-plane. Panels (a2)/(b2) show the equilibria in (A, B, Y)-space, where the mixed-mode periodic orbit from Figure 4 for $k_6 = 10^{-5}$ and $k_6 = 0$ has been superimposed. The direction of the flow towards and away from the (A, B)-plane changes direction, as indicated by arrows in Figure 5, when the hyperplane $\Sigma^{\perp} = \{(A, B, X, Y) \,|\, B = k_4/k_1\}$ is crossed. This condition follows from the Jacobian for (3)–(4) for $X = Y = 0$, which has the two eigenvalues $k_1 B - k_4$ and $-k_3 AB - k_5$ (in the direction normal to the (A, B)-plane) of which the latter is always negative. The $B = k_4/k_1 \approx 58.824$ condition is

exact for the case $k_6 = 0$ in panels (b), where the (A, B)-plane is invariant, but still describes the normal attraction/repulsion of the (A, B)-plane well for $k_6 = 10^{-5}$ in panels (a).

In Figure 5 there are several branches of equilibria. Those that are shown in black lie in the physically relevant quadrant where the concentrations X and Y satisfy $X \geq 0$, $Y \geq 0$. For the grey branches of equilibria, on the other hand, we have $X < 0$ or $Y < 0$. Although only positive values for the reactants are physically relevant in the Olsen model, all equilibria are interesting from the theoretical point of view, because they are important for the overall behavior of the system. Notice also the degree of symmetry of the two types of equilibrium branches with respect to $\Sigma^{\perp}$.

For small positive $k_6 = 10^{-5}$, as in Figure 5(a1), there is a single black and a single grey equilibrium branch. The black branch of physically relevant equilibria is stable where it is practically horizontal near $A = 8$. This equilibrium loses its stability at a saddle-node bifurcation S, which is characterized by a very sharp fold of the branch very close to $\Sigma^{\perp}$. The branch continues towards lower values of B and, after a second saddle-node bifurcation S at $B \approx 31.775$, regains stability in the subcritical Hopf bifurcation H at $B \approx 49.234$. The bifurcating family $\widehat{\Gamma}$ of unstable periodic orbits is shown in the bifurcation diagrams in Figure 5(a1)/(b1) by plotting the extrema in A of the oscillations. The branch ends in a homoclinic bifurcation when it reaches the saddle-equilibrium near $A = 8$. The practically horizontal part near $A = 8$ of the grey branch of equilibria is initially unstable, changes stability at a saddle-node bifurcation S (a sharp fold) very close to $\Sigma^{\perp}$, and is then stable until a Hopf bifurcation H. The branch remains unstable past a saddle-node bifurcation S and a further Hopf bifurcation H. Since they are not physically relevant, we do not show the families of periodic orbits that bifurcate from the grey branch of equilibria.

The bifurcation diagram for $k_6 = 0$ in Figure 5(b1) is very similar: the different branches of equilibria and the bifurcating family $\widehat{\Gamma}$ of periodic orbits appear to be identical. However, there is a difference in the bifurcation structure of the equilibria near $(A, B) = (8, 58.824)$. Namely, for $k_6 = 0$ the (A, B)-plane is invariant, and the two fold bifurcations merge into a transcritical bifurcation (TC) that takes place exactly on the hyperplane $\Sigma^{\perp}$. There is now a single horizontal branch of equilibria, given by $A = k_7/k_{-7} = 8$ and $X = Y = 0$. Hence this entire branch is physically relevant and appears in black. The stability of the horizontal branch is determined only by the direction of the flow normal to the invariant (A, B)-plane: it is stable to the left of $\Sigma^{\perp}$ (for $B < k_4/k_1$) and unstable to the right of $\Sigma^{\perp}$ (for $B > k_4/k_1$). Overall, we conclude that the situation for small positive k_6 is qualitatively like that for the special case $k_6 = 0$, except that the transcritical bifurcation TC is unfolded into two saddle-node bifurcations S.

The three-dimensional plots in Figure 5(a2)/(b2) of (A, B, Y)-space show what the bifurcation diagram of the fast subsystem means in terms of the dynamics of MMOs in the full Olsen model, which features slow dynamics in B. Namely, also plotted are the respective mixed-mode periodic orbits from Figure 4 for $k_6 = 10^{-5}$ and $k_6 = 0$. These orbits show that small oscillations arise near the Hopf bifurcation point H, while the entry of the region to the right of $\Sigma^{\perp}$ (for $B > k_4/k_1$) triggers the return back to the vicinity of H. Indeed, the local and global aspects of MMOs are clearest for the case $k_6 = 0$ in Figure 5(b2), on which we concentrate now. The mixed-mode periodic orbit Γ in panel (b2) is composed of a slow passage through the Hopf point H of the physically relevant equilibria: the trajectory approaches the stable part of the branch in a spiralling fashion until H and then starts to

spiral away from the now unstable branch of (black) equilibria. This part of Γ has all the hallmarks of a classic delayed Hopf bifurcation [10, 25, 26]. Note that the number of small oscillations towards the attracting equilibrium is about the same as that away from the unstable equilibrium after the Hopf bifurcation. At $B \approx 40.75$ the trajectory moves away from the branch of equilibria, where it closely follows the flow on the invariant (A, B)-plane. This flow is the composition of an exponential approach of the horizontal equilibria in A with a constant drift to larger values of B, given by

$$\phi(t) = \left(\left[A_0 - \frac{k_7}{k_{-7}} \right] e^{-k_{-7}t} + \frac{k_7}{k_{-7}}, B_0 + k_8 t \right) \tag{5}$$

for initial condition (A_0, B_0). The part of Γ in the region where $B < k_4/k_1$, to the left of $\Sigma^{\perp}$, is attracted to the (A, B)-plane. After crossing $\Sigma^{\perp}$ the trajectory initially still stays close to the now unstable (A, B)-plane; this is another example of a delayed bifurcation. It then makes a large excursion where it appears to follow the unstable direction of a saddle equilibrium on the horizontal branch of equilibria for $B > k_4/k_1$. As a result, there is reinjection back to a neighborhood of the attracting branch, and the process of slow passage through the Hopf bifurcation repeats.

4 Slow manifolds of the Olsen model

Figure 5 already hints at how geometric properties of the flow of system (1)–(4) give rise to MMOs. Our main goal now is to understand and illustrate this geometry in more detail by considering and computing suitable attracting and repelling surfaces that organize the dynamics, where we concentrate on the case $k_6 = 0$. This approach is motivated by our previous studies of attracting and repelling slow manifolds near a folded node in a three-dimensional phase space [7, 8]; see also [12, 31]. The difficulty here is that the Olsen model (1)–(4) is of dimension four and lacks a clear separation of time scales, so that it is not immediately clear which surfaces one should study. The main idea is to define surfaces in (A, B, Y)-space as manifolds associated with stable and unstable directions of saddle equilibria, and to extend them in such a way that their interaction near the Hopf bifurcation H gives useful information on the nature of MMOs in the full Olsen model. Our choice of attracting and repelling surfaces is informed directly by the bifurcation structure presented in Figure 5. Furthermore, it agrees with observations in [5, 19] of properties of the dynamics of (1)–(4) in different parts of phase space.

We first consider the surface S^r_B, which we will refer to as the repelling slow manifold. It is defined as the one-parameter family of stable manifolds of the equilibria of the fast subsystem (where $\alpha = 0$) that lie between the left saddle-node bifurcation point S (of the physically relevant equilibrium) and the plane $\Sigma^{\perp}$ in Figure 5(b1). However, in system (1)–(4) for $\alpha = 0$ these saddle equilibria have two-dimensional stable manifolds. Therefore, we make a further reduction step by a quasi steady-state approximation (QSSA). This technique is standard in chemical dynamics [11] and assumes that a reactant reaches its equilibrium value so fast that it can be considered, in first approximation, as constant. Hence, it can be replaced by its equilibrium value, so that the phase space dimension is reduced by one. We

apply QSSA to the variable X, which is then given by

$$X = \frac{k_1 B - k_4 + \sqrt{(k_1 B - k_4)^2 + 8k_2(3k_3 ABY + k_6)}}{4k_2}. \tag{6}$$

The QSSA-reduced fast subsystem of the Olsen model is given by the equations (1) for A and (4) for Y, where B is a parameter. For fixed B the stable manifold of the saddle equilibrium of the QSSA-reduced fast subsystem lies in the (A, Y)-plane and is of dimension one. It spirals onto the repelling equilibrium for $B \in [31.775, 49.234]$ (between the left-most saddle-node bifurcation S and the Hopf bifurcation H) and onto the repelling periodic orbit for $B \in [49.234, 54.779]$ (between the Hopf bifurcation H and the homoclinic bifurcation). The repelling slow manifold S^r_B is defined as the B-family of these one-dimensional stable manifolds, and it can be thought of as organizing how an orbit leaves the vicinity of the unstable equilibrium after the slow passage through the Hopf point H. The surface S^r_B can readily be computed as a one-parameter family of orbit segments starting on the respective linear stable eigenspaces at a small distance from the saddle equilibria. This computation was performed with the collocation routine of AUTO [2] by defining a suitable two-point boundary value problem. Here the orbit segment that one continues in B can be specified either by fixing its total integration time or by restricting its other endpoint to a suitable section; see also [16, 17].

To define the surface S^a_B, which we refer to as the attracting slow manifold, we consider the family of unstable manifolds of the saddle-type horizontal equilibria for $A = 8$ and $B > k_4/k_1$ in Figure 5(b1). In the slow subsystem, where B is a parameter, these equilibria have one-dimensional unstable manifolds, so that this B-dependent family forms a two-dimensional surface. (Hence, no further reduction with QSSA is needed.) Specifically, for fixed $B > k_4/k_1$ the unstable manifolds lie in the (A, X, Y)-space and, after a first large excursion, spiral towards the attracting equilibrium (for the same value of B). However, since B does not change, this resulting surface of unstable manifolds stays to the right of the plane $\Sigma^\perp$ so that it does not reach the vicinity of the Hopf point H. Therefore, we consider as the attracting slow manifold S^a_B the family of one-dimensional unstable manifolds in (A, B, X, Y)-space when B is allowed to vary, that is, when $\alpha = 1$. This has the effect that the two-dimensional surface S^a_B, after a first large excursion towards the stable branch is "pulled" through the vicinity of H by the slow drift in B. Hence, it interacts with the repelling slow manifold S^r_B as desired.

The computation of the surface S^a_B is necessarily more involved than that of S^r_B, but it can also be performed in a two-point boundary value problem setup with the collocation routine of AUTO [2]. To set up the computation three steps are required, which are very similar to those needed to compute a slow manifold near a folded node [7]. Throughout the entire computation we consider (a sequence of) well-posed numerical boundary value problems, so that existence and uniqueness of an isolated solution is guaranteed; see also [17]. The first step consists of computing an orbit segment $\mathbf{u}$ that approximates the one-dimensional unstable manifold in the fast subsystem (1)–(4) for $\alpha = 0$ for a chosen fixed value $B_0 > k_4/k_1$. This can be achieved by requiring that the begin point $\mathbf{u}(0)$ lies at a small distance on the linear unstable eigenspace of the saddle equilibrium and continuing in the integration time T until the orbit is sufficiently close to the attracting equilibrium. The next step is to "activate" the B-dynamics, which is achieved by continuation of $\mathbf{u}$ in the homotopy

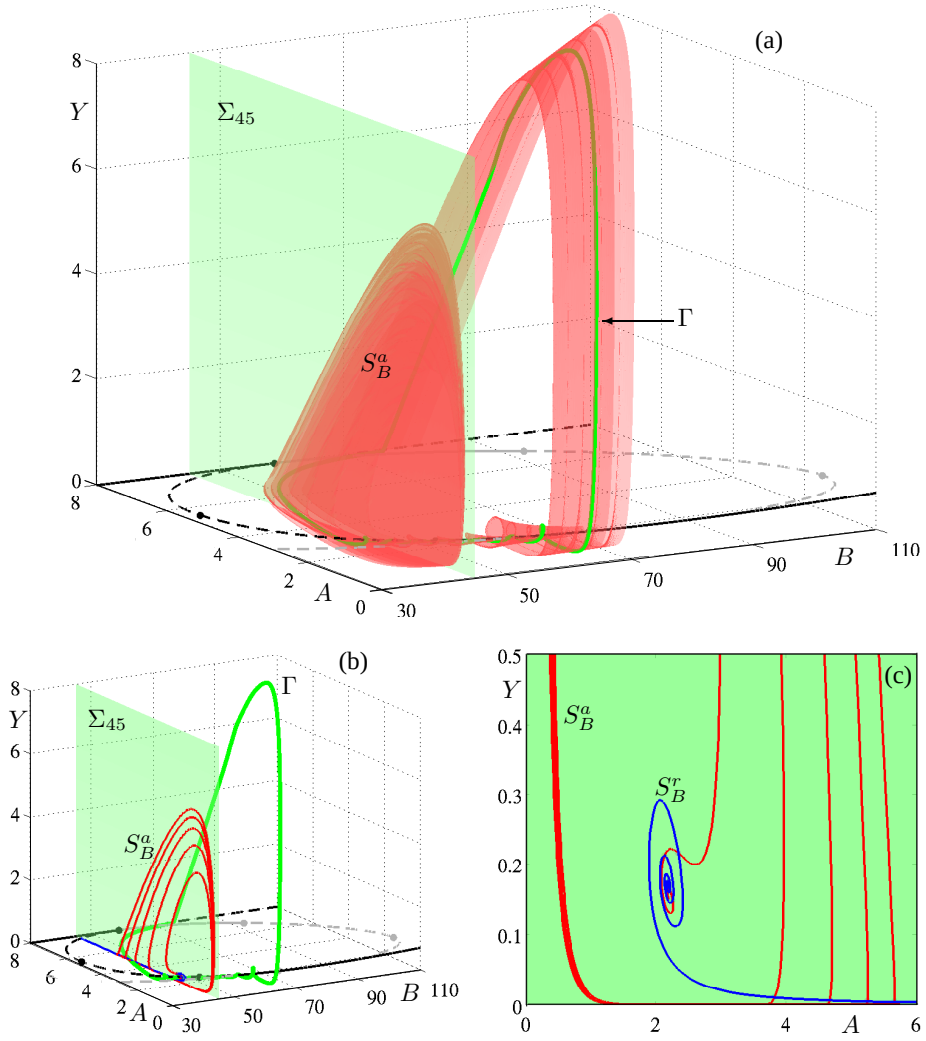

Figure 6: The attracting slow manifold S^a_B (red) of system (1)–(4) for $k_6 = 0$ (a), computed up to the section Σ_{45}. Panels (b) and (c) show the interaction of S^a_B with the repelling slow manifold S^r_B (blue) in Σ_{45}.

parameter α of (2) from 0 to 1 while keeping T fixed. As a result, the end point $\mathbf{u}(1)$ of the orbit segment moves along the branch of attracting equilibria, meaning that $\mathbf{u}(1)$ lies in the section $\Sigma_B(\alpha) = \{(A, B, X, Y) \,|\, B = B(\alpha)\}$. Hence, when $\alpha = 1$ has been reached at the end of this step, we have $\mathbf{u}(1) \in \Sigma_B(1)$ for some $B(1)$. The final step consists of moving the end point $\mathbf{u}(1)$ to lie in a suitable section to the left of the Hopf point H, which we choose here to be the section $\Sigma_{45} = \{(A, B, X, Y) \,|\, B = 45.0\}$. This can be achieved by continuation in the position B of the section Σ_B from $B = B(1)$ to $B = 45.0$, while requiring $\mathbf{u}(1) \in \Sigma_B$ and $\mathbf{u}(0)$ is fixed, and allowing T to vary. After this step the orbit segment $\mathbf{u}$ starts near the horizontal saddle equilibrium $(A, B, X, Y) = (8, B_0, 0, 0)$ and it ends in Σ_{45}. Hence, a part of interest of the two-dimensional surface S^a_B is swept out by continuation in the position B_0 of the unstable equilibrium, while requiring that $\mathbf{u}(1) \in \Sigma_{45}$. Note that during this

continuation the endpoint $\mathbf{u}(1)$ traces the one-dimensional intersection curve $S_B^a \cap \Sigma_{45}$.

Figure 6(a) illustrates the computation of S_B^a (red surface) from the horizontal line of saddle equilibria up to the section Σ_{45} (green plane). Also shown are the stable periodic attractor Γ (thick green orbit) and the curves of equilibria of the fast subsystem (1)–(4) for $\alpha = 0$ represented as in Figure 5 in black (grey) for the admissible (nonadmissible) quadrant. The very shape of the red surface S_B^a emphasizes the three main phases organizing the geometry of the associated mixed-mode periodic orbit Γ. Starting at maximal A, the family of orbit segments forming the red surface S_B^a first makes an excursion along the unstable eigendirection of the trivial saddle equilibrium. Then, orbits are strongly attracted towards the branch of stable equilibria of the fast subsystem and start spiralling around it while approaching the Hopf bifurcation point. The computation allows a good visualization of the slow passage through the Hopf point. Finally, the escape from the vicinity of the branch that has become unstable past the Hopf point, is organized via a rapid increase of the variable A. The periodic orbit Γ stays close to the invariant (A, B)-plane until, after crossing $\Sigma^{\perp}$, A is maximal again; see Figure 6(b). Also interesting from this picture are the different sheets that S_B^a develops in the vicinity of the escape region. These sheets correspond to successive excursions with increasing Y-amplitude. This explains the spiral that one can observe as the intersection of S_B^a with the cross-section Σ_{45}. Panels (b) and (c) focus on this intersection curve $S_B^a \cap \Sigma_{45}$ together with the corresponding intersection of the repelling slow manifold S_B^r (blue curve). Panel (b) still gives a three-dimensional view of Γ, the equilibrium curves of the fast subsystem and S_B^a in Σ_{45}; it also shows S_B^r but it is difficult to get a precise idea of the intersections of S_B^a and S_B^r in Σ_{45} due to the scaling. In order to understand this interaction of attracting and repelling slow manifolds in section Σ_{45}, panel (c) shows a two-dimensional image of the intersection curves in section Σ_{45}, enlarged in the region close to the invariant (A, B)-plane where both curves spiral. The intersection curve of S_B^r spirals out from an unstable focus of the fast subsystem and that of S_B^a winds around it one more time after each one of the large excursions shaping the multiple sheets of the red surface as observed in panel (a). The intersection points between S_B^a and S_B^r in Σ_{45} correspond to very specific orbits that locally organize the geometry of MMOs. These special orbits are described in the next section.

5 Canard-like orbits

By construction the attracting and repelling slow manifolds S_B^a and S_B^r allow us to illustrate how the global dynamics of the Olsen model works by considering the geometry of these surfaces only in (A, B, Y)-space. Starting from near a saddle equilibrium $(8, B_0, 0)$, the trajectory closely follows the attracting slow manifold S_B^a. That is, it makes a large excursion into the region of positive Y, approaches the stable equilibrium and then slowly drifts along it, finally passing the Hopf point H. Supposing that the trajectory reaches the section Σ_{45}, the dynamics away from the now unstable equilibrium is governed by the repelling slow manifold S_B^r. Namely, the orbit spirals around the equilibrium until it escapes through the region between S_B^r and the invariant (A, B)-plane. During this process the trajectory follows in good approximation the flow ϕ of (5) on this plane. In particular, the trajectory drifts in the B direction and towards the horizontal equilibria, while converging exponentially to the

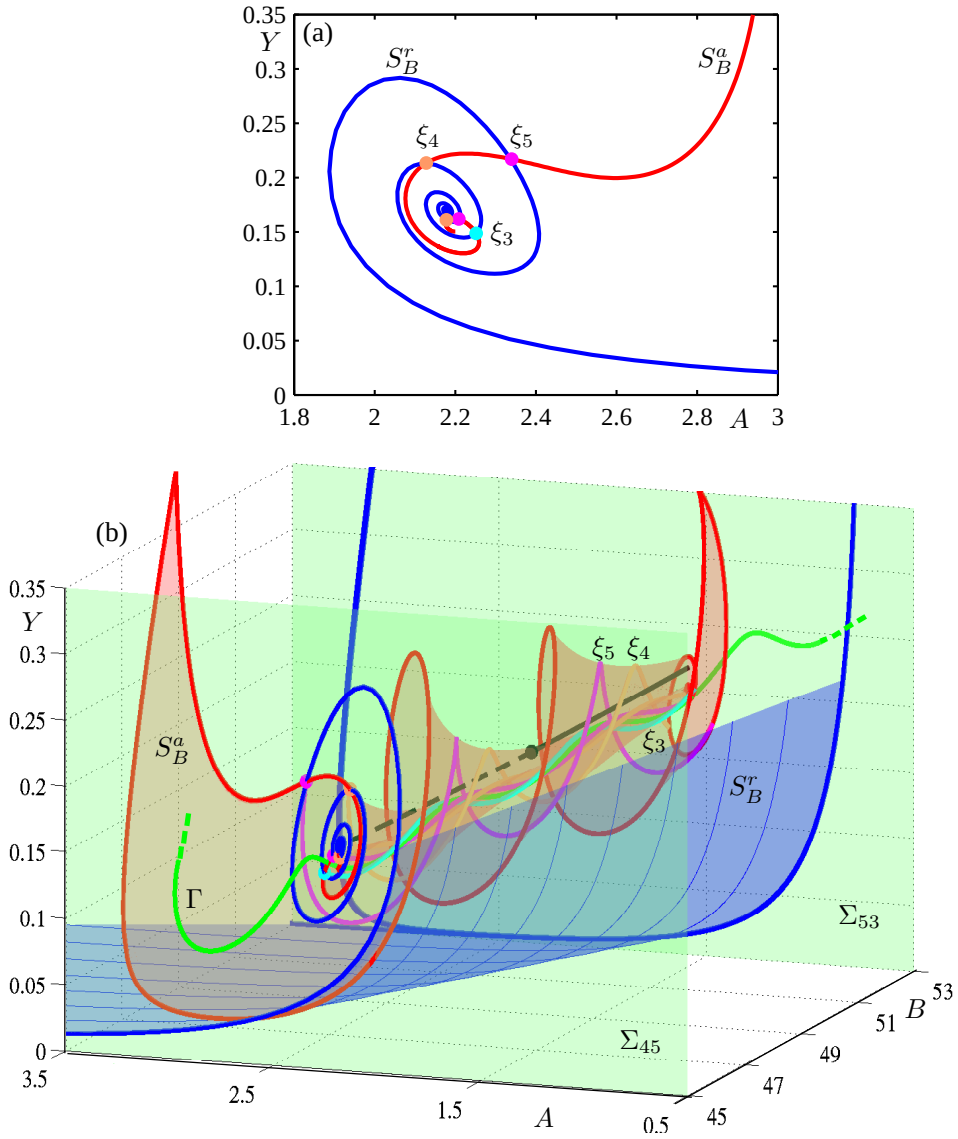

Figure 7: The curves S^a_B and S^r_B in Σ_{45} (a), and the surfaces S^a_B and S^r_B in (A, B, Y)-space in between the sections Σ_{45} and Σ_{53}. Also shown are five canard-like orbits ξ_1–ξ_5 that arise from the intersection of S^a_B and S^r_B in Σ_{45}.

(A, B)-plane until it crosses $\Sigma^{\perp}$. The trajectory then slowly diverges away from the (A, B)-plane. After some delay it makes the next large excursion back to the stable equilibrium, where the jump-off point is near some other saddle equilibrium $(8, B_1, 0, 0)$. Note that for the periodic orbit Γ in Figure 6 we have that $B_0 = B_1$. What is more, for the standard parameter values and $k_6 = 0$ the periodic orbit Γ is the only attractor, so that any trajectory converges to Γ.

Figure 7 illustrates the local interaction of S^a_B and S^r_B in the vicinity of the Hopf bifurcation H. Panel (a) shows the intersection curves of S^a_B and S^r_B with Σ_{45}. These two curves

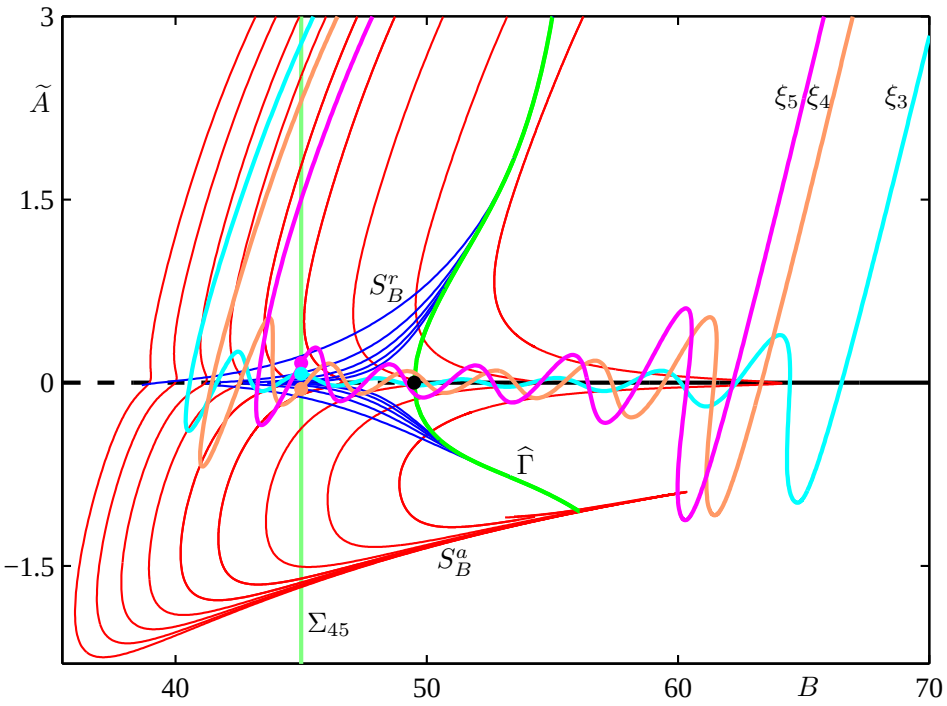

Figure 8: Passage of the canard-like orbits ξ_3–ξ_5 through the vicinity of the delayed Hopf bifurcation. Shown is the projection of ξ_3–ξ_5 onto the section $\Pi = \{(A, B, Y) \,|\, Y =\approx 0.00582B - 0.0911\}$, where the data is drawn relative to the curve of equilibria (which lie in Π); also shown are the intersection curves of the family of periodic orbits $\widehat{\Gamma}$ (green) and of the surfaces S^a_B (red) and S^r_B (blue) with Π; the vertical green line indicates the position of the section Σ_{45}.

spiral in opposite directions, and they intersect at five discrete points ξ_1–ξ_5. In analogy with canard orbits near a folded node [8, 12, 31], we refer to the trajectories through these points ξ_1–ξ_5 as canard-like orbits. Figure 7(b) shows the surfaces S^a_B and S^r_B, the canard-like orbits ξ_1–ξ_5 and the periodic orbit Γ in between the sections Σ_{45} and Σ_{53}. Notice that ξ_1–ξ_5 lie on the attracting slow manifold S^a_B, so that they are closely associated with the spiralling nature of trajectories locally near the delayed Hopf bifurcation. For a clear understanding of the different objects represented in this picture, we show the intersection curves of S^r_B with Σ_{45} and Σ_{53}, but the repelling slow manifold S^r_B itself is only computed up to the section $\Pi = \{(A, B, Y) \,|\, Y \approx 0.00582B - 0.0911\}$, which locally contains the equilibrium branch. Note that the canard-like orbits ξ_1–ξ_5 do not lie on S^r_B. This is because we defined the repelling slow manifold by considering the QSSA-reduced fast subsystem where B is a parameter. Hence, the ξ_1–ξ_5 depend on the choice of section, Σ_{45} in this case, which is why we refer to them as canard-like. Nevertheless, and as is also shown in Figure 7(b), the canard-like orbits locally define sectors of oscillations in this region of phase space, illustrating the nature of small-amplitude oscillations due to the slow passage near the Hopf bifurcation.

How the canard-like orbits organize the dynamics more globally is further illustrated in

Figure 8. The canard-like orbits ξ_3–ξ_5 are shown in projection onto the section Π, which contains the Hopf bifurcation and (locally) the curve of equilibria. Also shown are curves of intersection of S^a_B and S^r_B with Π, as well as the family $\widehat{\Gamma}$ of periodic orbits. To emphasize the relative positions of objects, we plot their A-distance $\widetilde{A}$ to the curve of equilibria, represented in Figure 8 as the B-axis. The vertical line is the section Σ_{45} that was used to define the canard-like orbits ξ_3–ξ_5. The repelling slow manifold S^r_B (computed for fixed $B \in [45, 53]$) intersects Π in curves that approach the union of the branch of unstable equilibria and the family $\widehat{\Gamma}$ of periodic orbits, which are also unstable. By contrast, the intersection curves of the attracting slow manifold S^a_B with the section Π form a layered structure, which corresponds to the multiple large excursions encountered in the transient dynamics of the system; compare with Figure 6(a). Note that the ξ_3–ξ_5 lie in different sectors defined by $S^a_B \cap \Pi$. Figure 8 shows that the number of oscillations during the slow passage through the Hopf bifurcation changes by one from one canard-like orbit to the next: namely, ξ_3 makes 7 rotations, ξ_4 makes 6 rotations and ξ_5 makes 5 rotations around the branch of equilibria. Hence, Figure 8 is evidence that canard-like orbits as introduced here indeed organize the rotations much like canard orbits associated with a folded node.

6 Discussion and outlook

We investigated how MMOs arise in the Olsen model for peroxidase-oxidase reaction, which is an ordinary differential equation for four reactants. We first presented a continuation study of mixed-mode periodic orbits, which revealed a complicated bifurcation structure with accumulating isolas and many regions of multistability between different types of MMOs. As a bifurcation analysis of the three-dimensional fast subsystem showed, MMOs in the Olsen model are characterized by a delayed Hopf bifurcation, which gives rise to small oscillations, in combination with a global reinjection mechanism that is responsible for large amplitude excursions. We then showed how (suitable parts of) attracting and repelling two-dimensional slow manifolds can be defined and computed that allow one to understand and illustrate the geometry that is responsible for MMOs. The main idea was to define the slow manifolds as stable and unstable manifolds of saddle equilibria of different reductions of the Olsen model. This approach allowed us to deal with the problem that it is of dimension four and the fact that it lacks a clear split into slow and fast variables. The attracting and repelling slow manifolds interact near the Hopf bifurcation of the fast subsystem, but also describe the geometry of the global reinjection mechanism. The spiralling nature of MMOs during the passage through the delayed Hopf bifurcation is locally organized by canard-like orbits.

The geometric numerical study presented here provides new insight into the nature of MMOs of the Olsen model, which naturally leads to quite a number of question for future research. First of all, we made use of the fact that the (A,B)-plane is invariant when the parameter k_6 is zero. However, as our bifurcation anlysis of mixed-mode periodic orbits for the standard value of $k_6 = 10^{-5}$ indicates, this property does not appear to be crucial. Our results suggest that the main global properties of the attracting and repelling slow manifolds — their interaction near a delayed Hopf bifurcation and the global reinjection mechanism — are preserved in a neighborhood of the standard parameter values. On the other hand, the MMOs themselves depend quite sensitively on parameters, and this has to do with the

exact local interaction of the slow manifolds near the Hopf bifurcation. The one-parameter bifurcation diagrams of mixed-mode periodic orbits presented here appear to be organized by an underlying global bifurcation of higher-codimension; specifically, the accumulation of isolas with cascades of period-doublings may be due to a nearby homoclinic doubling cascase [15, 27]. A natural next task is, therefore, a detailed bifurcation study of the mixed-mode periodic orbits in several parameters. Such a study would also shed some light on how the MMO patterns of large and small oscillations are organized.

Another question is how the global properties of the attracting and repelling slow manifolds may change with parameters. One possibility is that the bifurcation diagram of the equilibria of the fast subsystem changes in a codimension-two bifurcation, for example, a Bogdanov-Takens, saddle-node Hopf or degenerate transcritical bifurcation. Therefore, it is an interesting project to investigate how the delayed Hopf bifurcation and the global reinjection mechanism arise from the unfolding (in suitable parameters) of such codimension-two bifurcations of the fast subsystem.

Finally, we expect that our geometric approach will be useful for the analysis of other systems of moderate dimension whose slow-fast nature is not immediately obvious from the governing equations. The key is to identify regions of phase space where the flow is driven towards lower-dimensional slow manifolds, which hence, organize the dynamics locally and connect globally to an overall geometric structure. This point of view is similar to that behind the idea of reducing a slow-fast system to a hybrid system of lower-dimensional (return) maps and connecting flows [6, 12]. The difference is that the reduction to (noninvertible) maps "hardwires" the effect of dimension reduction in the fast limit, while we consider the geometry of the (invertible) flow on the entire phase space. It would be an interesting project to compare the two approaches by means of a case study. In particular, we believe that numerical methods as implemented in [6] may be of help for identifying slow manifolds in different regions of phase space.

Acknowledgements

We thank Martin Krupa for helpful discussion on the Olsen model. The work of M.D. was supported by EPSRC grant EP/C54403X/1, and that of H.M.O. by an EPSRC Advanced Fellowship grant.

References

[1] Baltazar D. Aguda, Raima Larter, and Bruce L. Clarke. Dynamic elements of mixed-mode oscillations and chaos in a peroxidase–oxidase model network. *The Journal of Chemical Physics*, 90(8):4168–4175, 1989.

[2] Eusebius J. Doedel, Randy C. Paffenroth, Alan R. Champneys, Thomas F. Fairgrieve, Yuri A. Kuznetsov, Bart E. Oldeman, Björn Sandstede, and Xiao J. Wang. AUTO2000: Continuation and Bifurcation Software for Ordinary Differential Equations. Available at `http://cmvl.cs.concordia.ca/`.

[3] Tatiana V. Bronnikova, William M. Schaffer, and Lars F. Olsen. Nonlinear dynamics of the peroxidase-oxidase reaction: I. bistability and bursting oscillations at low enzyme concentrations. *Journal of Physical Chemistry B*, 105(1):310–321, 2001.

[4] Morten Brøns, Martin Krupa, and Martin Wechselberger. Mixed mode oscillations due to the generalized canard phenomenon. In *Bifurcation theory and spatio-temporal pattern formation*, volume 49 of *Fields Inst. Commun.*, pages 39–63. Amer. Math. Soc., Providence, RI, 2006.

[5] Morten Brøns, and Martin Krupa. Mixed mode oscillations in the Olsen model for Peroxidase reaction. *SIAM Conference on Applications of Dynamical Systems*, Snowbird (Utah), 2007.

[6] Robert Clewley, Horacio G. Rotstein, and Nancy Kopell. A computational tool for the reduction of nonlinear ode systems possessing multiple scales. *Multiscale Modeling and Simulation*, 4(3):732–759, 2005.

[7] Mathieu Desroches, Bernd Krauskopf, and Hinke M. Osinga. Mixed-mode oscillations and slow manifolds in the self-coupled FitzHugh-Nagumo system. *Chaos*, 18(1):015107, 2008.

[8] Mathieu Desroches, Bernd Krauskopf, and Hinke M. Osinga. The geometry of slow manifolds near a folded node. *SIAM J. Appl. Dyn. Syst.*, to appear (2008).

[9] Hans Degn, Lars F. Olsen, and John W. Perram. Bistability, oscillation, and chaos in an enzyme reaction. *Annals of the New York Academy of Sciences*, 316(1):623–637, 1979.

[10] Steven M. Baer, Thomas Erneux, and John Rinzel. The slow passage through a Hopf bifurcation: delay, memory effects, and resonance. *SIAM J. Appl. Math.*, 49(1):55–71, February 1989.

[11] Simon J. Fraser. The steady state and equilibrium approximations: A geometrical picture. *The Journal of Chemical Physics*, 88(8):4732–4738, 1988.

[12] John Guckenheimer. Return maps of folded nodes and folded saddle-nodes. *Chaos*, 18(1):015108, 2008.

[13] Marcus J. Hauser and Lars F. Olsen. Mixed-mode oscillations and homoclinic chaos in an enzyme reaction. *J. Chem. Soc., Faraday Trans.*, 92(16):2857–2863, 1996.

[14] Marcus J. B. Hauser, Lars F. Olsen, Tatiana V. Bronnikova, and William M. Schaffer. Routes to chaos in the Peroxidase-Oxidase reaction: period-doubling and period-adding. *Journal of Physical Chemistry B*, 101(25):5075–5083, 1997.

[15] Ale Jan Homburg and Bernd Krauskopf. Resonant homoclinic flip bifurcations. *Journal of Dynamics and Differential Equations*, 12(4):807–850, 2000.

[16] Bernd Krauskopf, Hinke M. Osinga, Eusebius J. Doedel, Michael E. Henderson, John Guckenheimer, Alexander Vladimirsky, Michael Dellnitz, and Oliver Junge. A survey of methods for computing (un)stable manifolds of vector fields. *Internat. J. Bifur. Chaos*, 15(3):763–791, 2005.

[17] Bernd Krauskopf and Hinke M. Osinga. Computing invariant manifolds via the continuation of orbit segments. In B. Krauskopf, H. M. Osinga, and J. Galán-Vioque, editors, *Numerical Continuation Methods for Dynamical Systems: Path following and boundary value problems*, Underst. Complex Syst., pages 117–154. Springer-Verlag, New-York, 2007.

[18] Martin Krupa, Nikola Popović, Nancy Kopell, and Horacio G. Rotstein. Mixed-mode oscillations in a three time-scale model for the dopaminergic neuron. *Chaos*, 18(1):015106, 2008.

[19] Martin Krupa. Private communications, February 2008.

[20] Raima Larter, Christopher L. Bush, Timothy R. Lonis, and Baltazar D. Aguda. Multiple steady states, complex oscillations, and the devil's staircase in the peroxidase–oxidase reaction. *The Journal of Chemical Physics*, 87(10):5765–5771, 1987.

[21] Raima Larter and Curtis G. Steinmetz. Chaos via mixed-mode oscillations. *Philosophical Transactions: Physical Sciences and Engineering*, 337(1646):291–298, 1991.

[22] Raima Larter, Curtis G. Steinmetz, and Baltazar D. Aguda. Fast–slow variable analysis of the transition to mixed-mode oscillations and chaos in the peroxidase reaction. *The Journal of Chemical Physics*, 89(10):6506–6514, 1988.

[23] Georgi S. Medvedev and Jaime E. Cisternas. Multimodal regimes in a compartmental model of the dopamine neuron. *Physica D*, 194(3-4):333–356, 2004.

[24] Georgi Medvedev and Yun Yoo. Multimodal oscillations in systems with strong contraction. *Physica D*, 228(2):87–106, 2007.

[25] Anatoly I. Neĭshtadt. On stability loss delay for dynamical bifurcations I. *Differentsial' nye Uravneniya*, 23(12):2060–2067, (Russian); English translation in Differential Equations 23(12):1385–1390, 1987.

[26] Anatoly I. Neĭshtadt. On stability loss delay for dynamical bifurcations II. *Differentsial' nye Uravneniya*, 24(2):226–233, 364, (Russian); English translation in Differential Equations 24(2):171–176, 1988.

[27] Bart E. Oldeman, Bernd Krauskopf and Alan R. Champneys, Death of period-doublings: locating the homoclinic-doubling cascade, *Physica D*, 146(1-4):100–120, 2000.

[28] Lars F. Olsen. An enzyme reaction with a strange attractor. *Physics Letters A*, 94(9):454–457, 1983.

[29] William M. Schaffer, Tatiana V. Bronnikova, and Lars F. Olsen. Nonlinear dynamics of the peroxidase-oxidase reaction. II. compatibility of an extended model with previously reported model-data correspondences. *Journal of Physical Chemistry B*, 105(22):5331–5340, 2001.

[30] David R. Thompson and Raima Larter. Multiple time scale analysis of two models for the peroxidase–oxidase reaction. *Chaos*, 5(2):448–457, 1995.

[31] Martin Wechselberger. Existence and bifurcation of canards in $\mathbb{R}^3$ in the case of a folded node. *SIAM J. Appl. Dyn. Syst.*, 4(1):101–139, 2005.

[32] Isao Yamazaki, Kennosuke Yokota, and R. Nakajima. Oscillatory oxidations of reduced pyridine nucleotide by peroxidase. *Biochem. Biophys. Res. Commun.*, 21(6):582–586, 1965.

[33] Antonios Zagaris, Hans G. Kaper, and Tasso J. Kaper. Analysis of the computational singular perturbation reduction method for chemical kinetics. *Journal of Nonlinear Science*, 14(1):59–91, 2004.